Monte Carlo Shell Model and its Applications to Exotic Nuclei

Yutaka Utsuno

Advanced Science Research Center, Japan Atomic Energy Agency, 2-4 Shirakata-shirane, Tokai, Ibaraki 319-1195, Japan

Abstract

We give an overview of the development of the Monte Carlo shell model (MCSM). MCSM was originally based on the auxiliary-field Monte Carlo technique, but it is more like a stochastic variational method within multiple Slater determinants incorporating symmetry restoration. It is shown that complicated shell-model wave functions can be satisfactorily approximated with the MCSM calculation. MCSM has been applied to several cases, one of which is the neutron-rich region around $N = 20$, often called the island of inversion. A unified picture of the island of inversion is obtained with the MCSM calculations. The study of the island of inversion leads to a general concept of the shell evolution.

Keywords: *Shell model; Monte Carlo shell model; magic numbers; shell structure*

1 Introduction

Large-scale computing has been an indispensable tool in various fields of science. For instance, Japan has recently completed a new 10-PFlops supercomputer called K computer [1] in order to solve urgent problems in science and technology. Among various applications of the K computer, basic science including nuclear physics, has been regarded as one of the most important. In nuclear physics, large-scale computing enables one to describe nuclei from a more fundamental viewpoint. According to the forecast of Ref. [2], *ab initio* calculations in which a nucleus is built from nucleons interacting one with another via a bare nucleon-nucleon force only, will be extended to the *sd*-shell region in a near future. As for medium-heavy nuclei, the nuclear shell model, or the configuration interaction (CI) approach in terms of quantum chemistry, will be applicable up to the region around ^{132}Sn. Both methods need capability to deal with a huge number of many-body states. While exact calculation of the innumerable states such as the Lanczos diagonalization is developing accordingly, approximate methods should also be developed for surpassing the current limitation. The Monte Carlo shell model (MCSM) [3] is one of such methods, being developed to give a precise description of the CI problems with huge dimensionality. Its applicability is not limited to the conventional shell model which assumes an inert core and a relatively small number of valence orbits, but also includes *ab initio* calculations due to recent methodological and computational progress [4].

In this paper, we show some basics of MCSM and its early successful applications to the structure of exotic nuclei in the region near $N = 20$ which is often called "island of inversion" [5]. It is noted that a recent development of MCSM and a benchmark test for the *ab initio* calculation are presented in another paper [6]. We also show how the large-scale MCSM calculation plays an essential role in deeper understanding of exotic nuclei as exemplified by the so-called "shell evolution" that has been strongly motivated by the success of MCSM in the island of inversion.

2 Brief overview of the Monte Carlo shell model

The methodology of MCSM was proposed by Honma, Mizusaki and Otsuka in 1995 [7]. It is aimed at overcoming the limitation of CI due to huge dimensionality. It is noted that the first application was not the shell model but was the Interacting Boson Model (IBM). The computational method employed by MCSM is named the Quantum Monte Carlo Diagonalization (QMCD). QMCD was hinted by the shell model Monte Carlo (SMMC) method [8]. Thus, we first introduce basic ideas of SMMC in Sect. 2.1, and then present the QMCD method in Sect. 2.2.

2.1 SMMC: an auxiliary-field Monte Carlo method for the shell model

In general, the ground state of a quantum many-body system with the Hamiltonian H can be obtained, in principle, as

$$\exp(-\beta H)|\Phi\rangle \tag{1}$$

with $\beta \to \infty$ for any state $|\Phi\rangle$ that is not orthogonal to the ground state. However, in practice, a direct operation of $\exp(-\beta H)$ is almost impossible for a general Hamiltonian including two-body terms or higher. On the other hand, according to Thouless theorem [9], the operation of $\exp(-\beta h)$ on a Slater determinant leads to another Slater determinant for a one-body operator h. This is the starting point of SMMC.

Let us then take a simple two-body operator $H = O^2$ with O being a one-body operator. In this case, $\exp(-\beta H)$ is analytically expressed as

$$\exp(-\beta H) = \int_{-\infty}^{\infty} d\sigma \sqrt{\beta/\pi} \exp(-\beta\sigma^2 - 2\beta\sigma O). \tag{2}$$

Since any two-body operator disappears in Eq. (2), Eq. (1) can be computed for a Slater determinant $|\Phi\rangle$. For an arbitrary two-body operator H, a similar expression is obtained but is associated with more integration variables, which prevent one from directly performing the integration in practice. On the other hand, the integration can be practically carried out by using the Monte Carlo sampling. This is the essence of the so-called auxiliary-field Monte Carlo method where the integral variable σ is called the auxiliary field. The SMMC method [8] is based on this technique.

Although SMMC is suitable for studying properties of ground states and of systems at finite temperature, it is not so for properties of discrete excited levels. In addition, SMMC suffers from the sign problem for general two-body operators. These shortcomings are the motivation to develop another method called QMCD.

2.2 MCSM: application of the Quantum Monte Carlo Diagonalization method to the shell model

In the SMMC method, observables are obtained by using the Monte Carlo integration. In the QMCD method instead, a many-body wave function is obtained by using the diagonalization of the Hamiltonian in which basis states are generated by following the Monte Carlo sampling. This is the original idea of QMCD, and its efficiency has been demonstrated with an IBM Hamiltonian [7].

Once the many-body wave function is calculated with a finite number of basis states, it follows the variational principle. Namely, the energy of this wave function must be higher than the exact energy of the lowest state. In addition, the exact wave function must have good quantum numbers due to the symmetry of the Hamiltonian. Thus, keeping a stochastic procedure, the QMCD method has been developed to

directly utilize those properties. QMCD has adopted the projection technique in Ref. [10], and has been applied to the shell model in Ref. [11].

In the late 1990s, MCSM, the application of the QMCD method to the shell model, has been rather close to the present form and has been applied to systems beyond the limit of the exact diagonalization at that time [12]. Here, the formulation of MCSM is presented briefly. The many-body wave function of MCSM having total angular momentum J and its z component M is expressed as

$$|\Psi_{JM}\rangle = \sum_{k=1}^{N_{\rm MCSM}} f^{(k)} P^{\pi} \sum_{K=-J}^{J} g_K^{(k)} P^J_{MK} |\Phi(D^{(k)})\rangle, \tag{3}$$

where P^{π} and P^J_{MK} are the parity and angular-momentum projectors. $g_K^{(k)}$ denotes the mixing amplitude of the state having the intrinsic K and the basis index k. $f^{(k)}$ is the mixing amplitude for the k-th basis state (Slater determinant[1]) $|\Phi(D^{(k)})\rangle$ defined as

$$|\Phi(D^{(k)})\rangle = \prod_l \left(\sum_i D^{(k)}_{il} c^{\dagger}_i \right) |-\rangle. \tag{4}$$

In this expression, $g_K^{(k)}$, $f^{(k)}$ and $D^{(k)}_{il}$ are the parameters to be determined. Once all the $D^{(k)}_{il}$ are fixed, $g_K^{(k)}$ and $f^{(k)}$ that follows the variational principle are easily calculated by the diagonalization of the Hamiltonian. On the other hand, it is not straightforward to obtain the optimum form of each basis state, $D^{(k)}_{il}$.

In the MCSM calculation, $D^{(k)}_{il}$ are determined as follows. The number of the basis states, $N_{\rm MCSM}$, increases step by step: only $D^{(k)}_{il}$ of the last basis with $k = N_{\rm MCSM}$ can be varied at a time. The other $D^{(k)}_{il}$ with $k \leq N_{\rm MCSM}$ are kept unchanged. As for determining $D^{(k=N_{\rm MCSM})}_{il}$, at first, initial candidates are generated according to the Monte Carlo sampling using the auxiliary field σ (see Eq. (2)), and the $\sigma \mapsto D_{il}$ that gives the lowest energy is selected. The total energy labeled by σ is denoted as $E(\sigma)$. Next, around this σ, a small variation $\delta\sigma$ is applied. If $E(\sigma + \delta\sigma) < E(\sigma)$ is satisfied, $\sigma + \delta\sigma$ is adopted as the new σ. Otherwise, this $\sigma + \delta\sigma$ is discarded. This process is repeated until $E(\sigma)$ is saturated.

When the number of the basis states $N_{\rm MCSM}$ increases, the energy is lowered. The lowering of the energy at each increment becomes very small as the wave function is close to the eigenstate. Hence, the number of basis states $N_{\rm MCSM}$ increases until the energy is well converged. $N_{\rm MCSM}$ is typically several tens to hundred even though the dimension of the shell-model Hamiltonian is very large. In fact, it has been demonstrated that the ground-state energy of ^{56}Ni in the full pf-shell calculation with 1 billion M-scheme dimension is very well approximated by about 100 basis states in MCSM [12, 14].

3 MCSM description of the island of inversion

After the feasibility of MCSM was confirmed with some benchmark studies for the pf-shell calculation as shown in the last section, MCSM has been applied to cases where the exact diagonalization was impossible at that time. The neutron-rich region around $N = 20$, often referred to as the "island of inversion" [5], is one of the most successful applications of MCSM. The island of inversion is known as a region, including ^{32}Mg, where a strong deformation occurs in spite of the neutron magic number $N = 20$. The nuclei in the island are considered to be dominated by the $2p$-$2h$ excitation across the $N = 20$ shell gap. The dominance of the $2p$-$2h$ state is caused by energy gain due to

[1]For different form of the basis state, the pair-condensed basis has been used for a description of medium-heavy nuclei [13].

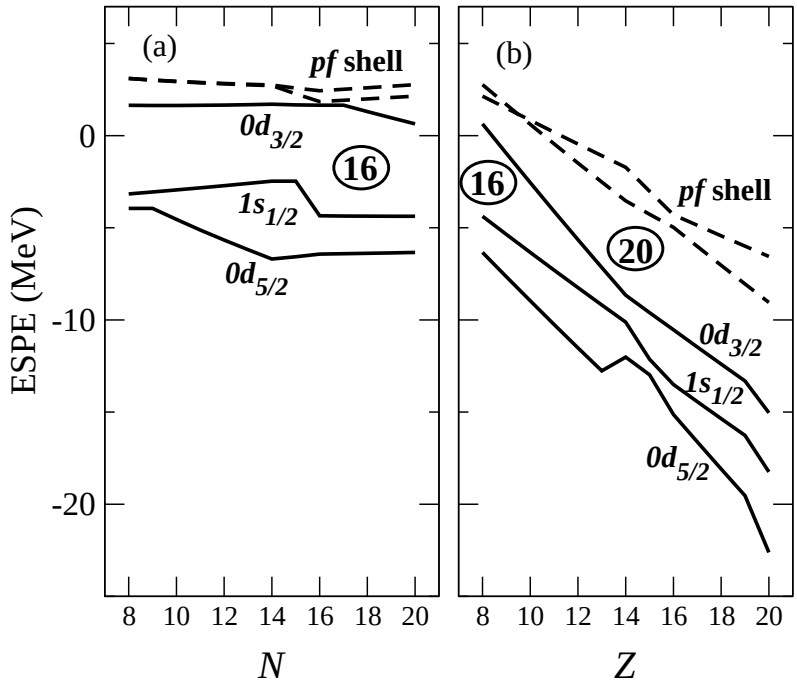

Figure 1: The neutron effective single-particle energies for (a) oxygen isotopes from $N = 8$ to 20 and (b) $N = 20$ isotones from $Z = 8$ to 20. See Ref. [3] for details . For the definition of the effective single-particle energy, see Ref. [15].

correlation or deformation that is larger than the energy loss of the spherical single-particle energy. Thus, accurate calculation of the correlation energy is needed for the description of the island of inversion.

Although the shell model is suitable for calculating the correlation energy, its application to the island of inversion was a difficult task due to the numerical limit of exact diagonalization. In order to describe excitation of nucleons from the sd to pf shell, the full sd shell and part of the pf shell should be included as the valence shell. Even if the pf shell is truncated up to $0f_{7/2}$ and $1p_{3/2}$, the number of single-particle states (including the degeneracy of j_z) reaches 24, which is larger than that of the full pf shell. For instance, the $M = 0$ dimension of ^{32}Mg in the $sd + f_{7/2} + p_{3/2}$ valence shell is larger than 10^9, which is beyond the computational limit in the early 2000s.

Thus, MCSM was best fitted for the shell-model calculation of the island of inversion. Taking the advantage of MCSM that is applicable to any nucleus on the same footing, we have succeeded in obtaining a unified picture for the $N = 20$ region ranging from stable to unstable nuclei [15]. As mentioned above, the shell gap is one of the most important ingredients for the theoretical framework. We have proposed a neutron shell structure which strongly changes from a smaller to a larger Z as presented in Fig. 1. Whereas the $N = 20$ shell gap is large for stable nuclei around ^{40}Ca, it is sharply reduced for lower Z. Instead of the disappearance of the normal $N = 20$ magicity, a new $N = 16$ magic structure appears near oxygen isotopes. This strong change of the shell structure was phenomenologically introduced in the shell-model Hamiltonian named SDPF-M [15] so that the drip line of oxygen isotopes, $N = 16$, can be reproduced with the shell-model calculation. In Ref. [15], a systematic calculation of yrast states of even-even nuclei has been carried out, demonstrating good agreement with the experimental energy levels and the $B(E2)$ values.

According to the varying shell gap shown in Fig. 1, the $N = 20$ shell gap is rather reduced for nuclei in the island of inversion with $Z = 10-12$. This helps those nuclei

to be dominated by the $2p$-$2h$ configurations. When the shell gap is reduced, it is expected that the extent of the island of inversion is enlarged. Thus, investigating the boundary of the island is of a great interest for probing the quenching of the shell gap proposed in Ref. [15]. This has been conducted with a systematic calculation of neutron-rich sodium isotopes ($Z = 11$) in Ref. [16]. In sodium isotopes, although electromagnetic moments of the ground states were known, their dominant configurations were not clear due to the lack of precise nuclear-structure calculations such as the shell model. The MCSM calculation has clarified that the $2p$-$2h$ dominance takes place at $N = 19$ from comparison between theoretical and experimental moments [16], enlarging the extent of the island of inversion from the original map [5]. It has been also demonstrated that this early onset of the $2p$-$2h$ dominance occurs only with a Hamiltonian having a reduced $N = 20$ shell gap. Thus, exotic properties of neutron-rich nuclei around $N = 20$ are successfully accounted for by the sharp change of the shell structure from stable to unstable nuclei.

4 Shell evolution

In Sec. 3, guided by large-scale shell-model calculations with MCSM, a strongly varying shell structure was phenomenologically introduced. Its origin and universality were not clear. After the MCSM study of the island of inversion, the understanding of the evolution of the shell structure, often called shell evolution, has been advanced. Thus, the shell evolution is one of good examples that a large-scale nuclear structure calculation leads to a deeper understanding of the nuclear structure from the fundamental point of view. In the following, a brief overview about the shell evolution is presented on the basis of our works.

As for the single-particle structure shown in Fig. 1, what causes the shift of magicity is the strong lowering of the neutron $0d_{3/2}$ orbit as protons occupy the $0d_{5/2}$ orbit. This is a consequence of a strong attraction between a proton in $0d_{5/2}$ and a neutron in $0d_{3/2}$. Since those two orbits are opposite in spin direction, the nuclear force dependent on spin seems to be essential. In Ref. [17], we have pointed out that the spin dependent central force can explain this strong attraction, generalizing a strong $T = 0$ attraction between the $j_>$ orbit and the $j_<$ orbit, where $j_>$ and $j_<$ stand for the orbits whose j's are $l + 1/2$ and $l - 1/2$, respectively. Indeed, realistic p-shell and pf-shell interactions have a strong attraction between $0p_{1/2}$ and $0p_{3/2}$ and between $0f_{5/2}$ and $0f_{7/2}$, respectively. As a result of this property, a new $N = 34$ magic number has been predicted in the neutron-rich calcium region.

Further study has clarified that the origin of this spin dependence is the tensor force [18], while the spin dependence of the central force plays a minor role. The tensor force gives the strong attraction between $j_>$ and $j'_<$ orbits even with different orbital angular momenta l and l'. The tensor force thus works to change the spin-orbit splitting. The *effective* tensor force turns out to be very close to the bare $\pi + \rho$ exchange force. This finding is based on comparison with experiment [18] and also on the analysis of the microscopic effective interaction [19, 20] using the spin-tensor decomposition [21]. It has also been found recently that the monopole part of the interaction, which is responsible for the shell evolution, after subtracting the tensor part is well simulated by a simple Gaussian force [19]. The tensor-subtracted effective interaction includes various effects such as a renormalization of the model space and the effect of the three-body force. Nonetheless, its monopole part can be well described by a simple interaction in terms of phenomenology. The reason for the validity of the Gaussian central force is yet to be clarified. The interaction consisting of the $\pi + \rho$ tensor force and the Gaussian central force seems to describe the shell evolution in a wide range of the nuclear chart, being named the monopole-based universal interaction ($V_{\rm MU}$) [19]. It has been shown that the phenomenological shell evolution of Fig. 1 is followed by the $V_{\rm MU}$ interaction.

Quite recently, $V_{\rm MU}$ has been applied to the effective interaction of the shell-model calculation in the neutron-rich region around $N = 28$ [22]. Using the shell-model calculation, we are able to discuss the shell evolution beyond the framework of the single-particle state. It is shown that the distribution of the spectroscopic factors for one-proton removal from ^{48}Ca is excellently reproduced by a Hamiltonian based on $V_{\rm MU}$. This result indicates that the proton spin-orbit splitting is strongly reduced from $N = 20$ to 28 by the tensor force, and that the reduction is quantitatively reproduced with $V_{\rm MU}$ including the $\pi + \rho$ tensor force. It is also shown that a very neutron-rich nucleus ^{42}Si is strongly oblate deformed because of quenching of proton sub-shell gaps induced by the tensor force. This deformation accounts for the low 2_1^+ state in ^{42}Si measured recently [23].

5 Summary

In summary, this paper reports a brief overview of the development of the Monte Carlo shell model (MCSM) and its earliest successful application to the neutron-rich region around $N = 20$. The shell evolution due to the effective interaction, an idea following the success of the MCSM calculation, is also presented. In the present paper, we stress that the development of large-scale nuclear-structure calculation leads not only to a quantitative description of various nuclei from a fundamental point of view but also to the construction of a new paradigm of nuclear physics.

Acknowledgment

The author is indebted to T. Otsuka, T. Mizusaki, M. Honma, N. Shimizu and T. Abe for a long term collaboration which constitutes the basis of this paper. He also acknowledges a collaboration with B. A. Brown for the shell-model study around $N = 28$. The study of this paper is in part supported by MEXT/JSPS KAKENHI Grant Numbers (13002001), (14740176), (17740165), and (21740204), and supported also by HPCI Strategic Program Field 5.

References

[1] K computer, http://www.aics.riken.jp/en/.

[2] SciDAC Review, Issue 6, p. 42 (2007).

[3] T. Otsuka, M. Honma, T. Mizusaki, N. Shimizu and Y. Utsuno, Prog. Part. Nucl. Phys. **47**, 319 (2001).

[4] N. Shimizu, T. Abe, Y. Tsunoda, Y. Utsuno, T. Yoshida, T. Mizusaki, M. Honma and T. Otsuka, Prog. Theor. Exp. Phys. **2012**, 01A205 (2012).

[5] E. K. Warburton, J. A. Becker and B. A. Brown, Phys. Rev. C **41**, 1147 (1990).

[6] T. Abe, P. Maris, T. Otsuka, N. Shimizu, Y. Utsuno and J. P. Vary, in *Proc. Int. Workshop Nucl. Theor. Supercomputing Era (NTSE-2012), Khabarovsk, Russia, June 18–22, 2012*, edited by A. M. Shirokov and A. I. Mazur. Pacific National University, Khabarovsk, 2013 (*see this book*), p. 33.

[7] M. Honma, T. Mizusaki and T. Otsuka, Phys. Rev. Lett. **75**, 1284 (1995).

[8] S. E. Koonin, D. J. Dean and K. Langanke, Phys. Rep. **278**, 1 (1997).

[9] D. J. Thouless, Nucl. Phys. **21**, 225 (1960).

[10] T. Mizusaki, M. Honma and T. Otsuka, Phys. Rev. C **53**, 2786 (1996).

[11] M. Honma, T. Mizusaki and T. Otsuka, Phys. Rev. Lett. **77**, 3315 (1996).

[12] T. Otsuka, M. Honma and T. Mizusaki, Phys. Rev. Lett. **81**, 1588 (1998).

[13] N. Shimizu, T. Otsuka, T. Mizusaki and M. Honma, Phys. Rev. Lett. **86**, 1171 (2001).

[14] K. W. Schmid, Prog. Part. Nucl. Phys. **52**, 565 (2004).

[15] Y. Utsuno, T. Otsuka, T. Mizusaki and M. Honma, Phys. Rev. C **60**, 054315 (1999).

[16] Y. Utsuno, T. Otsuka, T. Glasmacher, T. Mizusaki and M. Honma, Phys. Rev. C **70**, 044307 (2004).

[17] T. Otsuka, R. Fujimoto, Y. Utsuno, B. A. Brown, M. Honma and T. Mizusaki, Phys. Rev. Lett. **87**, 082502 (2001).

[18] T. Otsuka, T. Suzuki, R. Fujimoto, H. Grawe and Y. Akaishi, Phys. Rev. Lett. **95**, 232502 (2005).

[19] T. Otsuka, T. Suzuki, M. Honma, Y. Utsuno, N. Tsunoda, K. Tsukiyama and M. Hjorth-Jensen, Phys. Rev. Lett. **104**,

[20] N. Tsunoda, T. Otsuka, K. Tsukiyama and M. Hjorth-Jensen, Phys. Rev. C **84**, 044322 (2011).

[21] M. K. Kirson, Phys. Lett. **47B**, 110 (1973).

[22] Y. Utsuno, T. Otsuka, B. A. Brown, M. Honma, T. Mizusaki and N. Shimizu, arXiv:1210.5469 [nucl-th] (2012); to be published in Phys. Rev. C.

[23] B. Bastin *et al.*, Phys. Rev. Lett. **99**, 022503 (2007).

Application of the Monte Carlo Shell Model to *Ab Initio* No-Core Calculations

T. Abe[a], P. Maris[b], T. Otsuka[a,c,d], N. Shimizu[c], Y. Utsuno[e] and J. P. Vary[b]

[a] *Department of Physics, the University of Tokyo, Hongo, Tokyo 113-0033, Japan*
[b] *Department of Physics and Astronomy, Iowa State University, Ames, Iowa 50011, USA*
[c] *Center for Nuclear Study, the University of Tokyo, Hongo, Tokyo 113-0033, Japan*
[d] *National Superconducting Cyclotron Laboratory, Michigan State University, East Lansing, Michigan 48824, USA*
[e] *Advanced Science Research Center, Japan Atomic Energy Agency, Tokai, Ibaraki 319-1195, Japan*

Abstract

We report recent developments of the Monte Carlo Shell Model (MCSM) and its application to the no-core calculations. It is shown that recent developments enable us to apply the MCSM to the shell-model calculations without a core. Benchmarks between the MCSM and Full-Configuration Interaction (FCI) methods demonstrate consistent results with each other within estimated uncertainties. No-Core Full Configuration (NCFC) results are also presented as full *ab initio* solutions extrapolated to the infinite basis limit.

Keywords: *Shell model; Monte Carlo shell model; ab initio approaches*

1 Introduction

One of the major challenges in nuclear physics is to understand nuclear structure and reactions from *ab initio* calculations. Such calculations have recently become feasible for nuclear many-body systems beyond $A = 4$ due to the rapid evolution of computational technologies. Together with the Green's Function Monte Carlo [1] and Coupled Cluster theory [2], the No-Core Shell Model (NCSM) is one of the relevant *ab initio* methods and has been emerging for about a decade. It is now available for the study of nuclear structure and reactions in the p-shell nuclei [3].

As the NCSM treats all the nucleons democratically, computational demands for the calculations explode exponentially as the number of nucleons increases. Current computational resources limit the direct diagonalization of the Hamiltonian matrix using the Lanczos algorithm to basis spaces with a dimension of around 10^{10}. In order to access heavier nuclei beyond the p-shell region with larger basis dimensions, many efforts have been devoted to the NCSM calculations. One of these approaches is the Importance-Truncated NCSM [4] where the model spaces are extended by using an importance measure evaluated using perturbation theory. Another approach is the Symmetry-Adapted NCSM [5] where the model spaces are truncated by the selected symmetry groups. Similar to these attempts, the no-core Monte Carlo Shell Model (MCSM) [6, 7, 8] is one of the promising candidates to go beyond the Full Configuration Interaction (FCI) method which is a different truncation of the basis states that commonly used in the NCSM.

In these proceedings, we focus on the latest application of the MCSM toward the *ab initio* no-core calculations, which has become viable recently with the aid of major developments in the MCSM algorithm [8, 9, 10] and also a remarkable growth in the computational power of state-of-the-art supercomputers. The overview of the benchmarks in the no-core MCSM is based on the results mostly presented in Refs. [7, 8].

2 MCSM

The MCSM has been developed mainly for conventional shell-model calculations with an assumed inert core [11]. Recently the algorithm and code itself have been heavily revised and rewritten so as to accommodate massively parallel computing environments [8, 9, 10]. In this section, we briefly overview the MCSM and introduce some of recent developements.

2.1 Brief overview

The MCSM approach [11] proceeds through a sequence of diagonalization steps within the Hilbert subspace spanned by the deformed Slater determinants in the HO single-particle basis as the selected importance-truncated bases. A many-body basis state $|\Psi^{J^\pi M}\rangle$ is a linear combination of non-orthogonal angular-momentum (J) and parity (π) projected deformed Slater determinants with good total angular momentum projection (M) as a stochastically selected basis,

$$|\Psi^{J^\pi M}\rangle = \sum_{n=1}^{N_b} f_n \sum_{K=-J}^{J} g_{nK} P^J_{MK} P^\pi |\phi_n\rangle, \tag{1}$$

where the deformed Slater determinant is $|\phi\rangle = \prod_{i=1}^{A} a_i^\dagger |-\rangle$ with the vacuum $|-\rangle$ and the creation operator $a_i^\dagger = \sum_{\alpha=1}^{N_{\rm sp}} c_\alpha^\dagger D_{\alpha i}$. $N_{\rm sp}$ is specified by the cutoff of the single particle orbits, $N_{\rm shell}$. One then stochastically samples the coefficient $D_{\alpha i}$ in all possible many-body basis states around the mean field solutions through the auxiliary fields and diagonalizes the Hamiltonian matrix within the subspace spanned by these bases N_b. Stochastically sampled bases are accepted so as to minimize the energy variationally. Therefore the MCSM can evade the so-called negative sign problem, which is the fundamental issue that cannot be avoided in quantum Monte Carlo methods. With increasing MCSM basis dimension, N_b, the ground state energy of a MCSM calculation converges from above to the exact value. The energy, therefore, always gives the variational upper bound in this framework.

An exploratory no-core MCSM investigation demonstrating a proof-of-the principle has been done for the low-lying states of the Berylium isotopes by applying the existing MCSM algorithm with a core to a no-core problem [6]. Recent improvements on the MCSM algorithm have enabled significantly larger calculations [8, 9, 10]. We adopt these improvements in the present work [7, 8].

2.2 Recent developments

Among the recently achieved developments of our MCSM algorithm [8, 9, 10], in this subsection, we focus on two improvements: (1) the efficient computation of the two-body matrix elements (TBMEs) for the most time-consuming part in our calculations [8, 9] and (2) the energy-variance extrapolation for our MCSM (approximated) results to the FCI (exact) ones [8, 10]. There are other improvements such as the conjugate gradient method in the process of the basis search and the re-ordering technique in the energy variance extrapolations. Because of space limitations, we refer for the details of these improvements to Refs. [8, 10].

2.2.1 Efficient computation of the TBMEs

One of the main issues in the shell-model calculations is to evaluate TBMEs efficiently. As the matrix for the TBMEs is sparse in general, the indirect-index (list-vector) method is usually adopted in the shell-model calculations by keeping the value of the non-zero matrix elements and their indices. However, it tends to give slow performance due to the irregular memory access patterns.

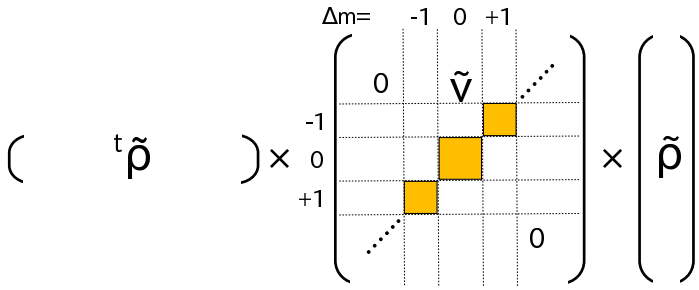

Figure 1: Schematic illustraion of the (vector)^t × (matrix) × (vector) operation.

Alternatively, in our recent MCSM code, we transform the sparse matrix to a block matrix with dense blocks by utilizing the symmetries of the two-body interaction [9]. The one-body density-matrix elements $\rho_{ll'}$ are grouped as $\tilde{\rho}(\Delta m)$ according to $\Delta m \equiv j_z(l') - j_z(l)$ where l and l' are the labels for the state. The TBMEs are also similarly categorized. Then, the two-body part of the Hamiltonian overlap can be expressed as schematically indicated in Fig. 1. Furthermore, most of the computational time is devoted to the (matrix) × (vector) operation. It is usually repeated a number of times for different $\tilde{\rho}$'s. By binding $N_{\rm vec}$ $\tilde{\rho}$-vectors into a matrix, repeated (matrix)×(vector) operations are replaced by a (matrix)×(matrix) operation at once. As shown in Fig. 2, we can achive 70−80 % of the peak performance with $N_{\rm vec} \sim 30-100$ in the test case of the (matrix) × (matrix) operation [9].

2.2.2 Energy-variance extrapolation to the FCI results

With increasing Monte Carlo basis dimension N_b, the MCSM results converge to the FCI results from above. In order to estimate the exact FCI answer, we extrapolate the energy and other observables evaluated by MCSM wave functions using the energy

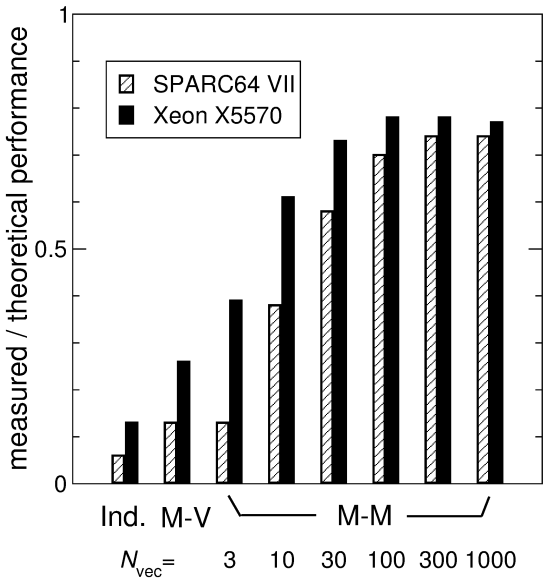

Figure 2: Comparison of the computational performance among the indirect-index method (Ind.), matrix-vector method (M-V) and matrix-matrix method (M-M) with different $N_{\rm vec}$ measured on the SPARC64 VII and Xeon X5570 systems. The values are normalized by their theoretical peak performance. See Ref. [9] for the details.

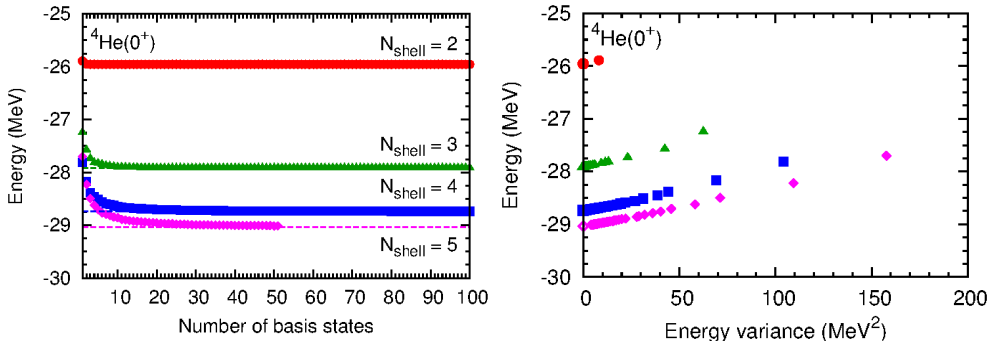

Figure 3: ^{4}He ground-state energies as functions of number of basis states (left) and energy variance (right). From the above to the bottom, the symbols (horizontal dashed lines in the left figure and open symbols at the zero energy variance in the right figure) are the MCSM (FCI) results in $N_{shell} = 2$, 3, 4 and 5, respectively. See Ref. [7] for the details.

variance [8, 10]. That is, the MCSM results are plotted as a function of the evaluated energy variance, $\Delta E_2 = \langle\Psi|H^2|\Psi\rangle - (\langle\Psi|H|\Psi\rangle)^2$, and then extrapolated to zero variance.

As a typical example, the behavior of the ground-state energies of ^{4}He (0^+) with respect to the number of basis states and to the energy variance are shown in Fig. 3. From Fig. 3, one can see that the MCSM results can be extrapolated to the FCI ones by using the quadratic fit function of $E(\Delta E_2) = E(\Delta E_2 = 0) + c_1\Delta E^2 + c_2(\Delta E_2)^2$ with the fitting parameters $E(\Delta E_2 = 0)$, c_1, and c_2.

3 Benchmarks

Augmented by the recent development of the MCSM algorithm [8, 9, 10], we have performed benchmarks of the no-core MCSM calculations [7, 8]. The main outcome of the initial benchmark project is summarized in Table 1. In Table 1, we illustrates the comparisons of the energies for each state and model space between the MCSM and FCI methods. The FCI gives the exact energies in the given model space while the MCSM gives approximate energies. Thus the comparisons between them show how well the MCSM works in no-core calculations. Furthermore, we also put the No-Core Full Configuration (NCFC) [12] results for the states of $4 \leq A \leq 10$ as the fully converged energies in the infinite model space.

For this benchmark comparison, the JISP16 two-nucleon interaction [13] is adopted and the Coulomb force is turned off. Isospin symmetry is assumed. The energies are evaluated for the optimal harmonic oscillator frequencies where the calculated energies are minimized for each state and model space. Here the contributions from the spurious center-of-mass motion are ignored for simplicity.

The comparisons are made for the states; ^{4}He (0^+), ^{6}He (0^+), ^{6}Li (1^+), ^{7}Li ($1/2^-$, $3/2^-$), ^{8}Be (0^+), ^{10}B (1^+, 3^+) and ^{12}C (0^+). The model space ranges from $N_{shell} = 2$ to 5 for $A \leq 6$ (4 for $A \geq 7$). Note that the energies of ^{10}B (1^+, 3^+) and ^{12}C (0^+) in $N_{shell} = 4$ are available only from the MCSM results. The M-scheme dimensions for these states are already close to or above the current limitation in the FCI approach. The numbers of basis states are taken up to 100 in $N_{shell} = 2{-}4$ and 50 in $N_{shell} = 5$.

As seen in Table 1, the energies are consistent with each other where the FCI results are available to within $\sim$ 100 keV ($\sim$ 500 keV) at most of the MCSM results with(out) the energy-variance extrapolation of the MCSM results. The other

Table 1: Energies in MeV calculated for seven ground states and two excited states within the MCSM and FCI methods using the JISP16 NN interaction. The entries of the MCSM indicate the MCSM results before the energy variance extrapolation, while those of the "extrp" line denote the MCSM results after the extrapolations. Uncertainties in extrapolated results are quoted in parenthesis. See Ref. [7] for the details.

		E (MeV)				
Nuclei	Method	$N_{\rm shell}=2$	3	4	5	NCFC
^{4}He	MCSM	-25.956	-27.914	-28.737	-29.011	-29.164(2)
(0^+)	extrp			-28.738(1)	-29.037(1)	
	FCI	-25.956	-27.914	-28.738	-29.036	
^{6}He	MCSM	-13.343	-19.186	-23.480	-25.080	-29.51(5)
(0^+)	extrp		-19.196(1)	-23.687(4)	-26.086(76)	
	FCI	-13.343	-19.196	-23.684	-26.079	
^{6}Li	MCSM	-14.218	-21.549	-26.757	-28.410	-33.22(4)
(1^+)	extrp		-21.581(1)	-27.166(16)	-29.873(83)	
	FCI	-14.218	-21.581	-27.168	-29.893	
^{7}Li	MCSM	-14.459	-24.073	-30.904		-39.8(1)
$(1/2^-)$	extrp		-24.167(2)	-31.780(51)		
	FCI	-14.458	-24.165	-31.748		
^{7}Li	MCSM	-17.232	-25.978	-32.494		-40.4(1)
$(3/2^-)$	extrp		-26.061(4)	-33.272(89)		
	FCI	-17.232	-26.063	-33.202		
^{8}Be	MCSM	-28.435	-41.242	-50.222		-59.1(1)
(0^+)	extrp		-41.293(1)	-50.753(32)		
	FCI	-28.435	-41.291	-50.756		
^{10}B	MCSM	-29.755	-41.965	-52.239		-68.5(1.5)
(1^+)	extrp		-42.357(46)	-54.89(16)		
	FCI	-29.755	-42.338			
^{10}B	MCSM	-34.221	-46.263	-56.346		-69.8(2)
(3^+)	extrp		-46.618(22)	-58.41(13)		
	FCI	-34.221	-46.602			
^{12}C	MCSM	-62.329	-76.413	-90.158		
(0^+)	extrp		-76.621(4)	-91.957(43)		
	FCI	-62.329	-76.621			

observables besides the energies; the point-particle root-mean-square matter radii and electromagnetic moments also give reasonable agreements between the MCSM and FCI results. The detailed comparisons among the MCSM, FCI, and NCFC methods are discussed in Ref. [7].

4 Summary

By exploiting the recent development in the efficient computation of the Hamiltonian matrix elements between non-orthogonal Slater determinants and the technique of energy-variance extrapolation, the observables give good agreement between the MCSM and FCI results in the p-shell nuclei. From the benchmark comparison, the no-core MCSM is now verified in the application to the *ab initio* no-core calculations for light nuclei. The application to heavier nuclei is expected in the near future.

Acknowledgments

This work was supported in part by the SPIRE Field 5 from MEXT, Japan. We also acknowledge Grants-in-Aid for Young Scientists (Nos. 20740127 and 21740204), for Scientific Research (Nos. 20244022 and 23244049), and for Scientific Research on Innovative Areas (No. 20105003) from JSPS, and the CNS-RIKEN joint project for large-scale nuclear structure calculations. This work was also supported in part by the US DOE Grants No. DE-FC02-07ER41457, DE-FC02-09ER41582 (UNEDF SciDAC Collaboration), and DE-FG02-87ER40371, by US NSF grand 0904782, and through JUSTIPEN under grant no. DE-FG02-06ER41407. A part of the MCSM calculations was performed on the T2K Open Supercomputer at the University of Tokyo and University of Tsukuba, and the BX900 Supercomputer at JAEA. Computational resources for the FCI and NCFC calculations were provided by the National Energy Research Supercomputer Center (NERSC), which is supported by the Office of Science of the U.S. Department of Energy under Contract No. DE-AC02-05CH11231, and by the Oak Ridge Leadership Computing Facility at the Oak Ridge National Laboratory, which is supported by the Office of Science of the U.S. Department of Energy under Contract No. DE-AC05-00OR22725.

References

[1] S. C. Pieper, R. B. Wiringa and J. Carlson, Phys. Rev. C **70**, 054325 (2004); K. M. Nollett, S. C. Pieper, R. B. Wiringa, J. Carlson and G. M. Hale, Phys. Rev. Lett. **99**, 022502 (2007).

[2] G. Hagen, M. Hjorth-Jensen, G. R. Jansen, R. Machleidt and T. Papenbrock, Phys. Rev. Lett. **108**, 242501 (2012); **109**, 032502 (2012) and references therein.

[3] P. Navrátil, J. P. Vary and B. R. Barrett, Phys. Rev. Lett. **84**, 5728 (2000); Phys. Rev. C **62**, 054311 (2000); S. Quaglioni and P. Navrátil, Phys. Rev. Lett. **101**, 092501 (2008); Phys. Rev. C **79**, 044606 (2009).

[4] R. Roth, Phys. Rev. C **79**, 064324 (2009); R. Roth, S. Binder, K. Vobig, A. Calci, J. Langhammer and P. Navrátil, Phys. Rev. Lett. **109**, 052501 (2012).

[5] T. Dytrych, K. D. Sviratcheva, C. Bahri, J. P. Draayer and J. P. Vary, Phys. Rev. Lett. **98**, 162503 (2007); J. Phys. G. **35**, 095101 (2008); T. Dytrych, K. D. Sviratcheva, J. P. Draayer, C. Bahri and J. P. Vary, *ibid.* **35**, 123101 (2008).

[6] L. Liu, T. Otsuka, N. Shimizu, Y. Utsuno and R. Roth, Phys. Rev. C **86**, 014304 (2012).

[7] T. Abe, P. Maris, T. Otsuka, N. Shimizu, Y. Utsuno and J. P. Vary, AIP Conf. Proc. **1355**, 173 (2011); Phys. Rev. C **86**, 054301 (2012).

[8] N. Shimizu, T. Abe, Y. Tsunoda, Y. Utsuno, T. Yoshida, T. Mizusaki, M. Honma and T. Otsuka, Prog. Theor. Exp. Phys. 01A205 (2012).

[9] Y. Utsuno, N. Shimizu, T. Otsuka and T. Abe, Comput. Phys. Comm. **184**, 102 (2013).

[10] N. Shimizu, Y. Utsuno, T. Mizusaki, T. Otsuka, T. Abe and M. Honma, Phys. Rev. C **82**, 061305(R) (2010); N. Shimizu, Y. Utsuno, T. Mizusaki, M. Honma, Y. Tsunoda and T. Otsuka, *ibid.* **85**, 054301 (2012).

[11] T. Otsuka, M. Honma, T. Mizusaki, N. Shimizu and Y. Utsuno, Prog. Part. Nucl. Phys. **47**, 319 (2001); Y. Utsuno, in *Proc. Int. Workshop*

Nucl. Theor. Supercomputing Era (NTSE-2012), Khabarovsk, Russia, June 18–22, 2012, edited by A. M. Shirokov and A. I. Mazur. Pacific National University, Khabarovsk, 2013 (*see this book*) p. 26.

[12] P. Maris, J. P. Vary and A. M. Shirokov, Phys. Rev. C **79**, 14308 (2009); P. Maris, A. M. Shirokov and J. P. Vary, *ibid.* **81**, 021301 (2010); C. Cockrell, P. Maris and J. P. Vary, *ibid.* **86**, 034325 (2010).

[13] A. M. Shirokov, J. P. Vary, A. I. Mazur and T. A. Weber, Phys. Lett. B **644**, 33 (2007); A. M. Shirokov, J. P. Vary, A. I. Mazur, S. A. Zaytsev and T. A. Weber, *ibid.* **621**, 96 (2005).